



# 1 Aerosol Mass yields of selected Biogenic Volatile Organic Compounds – a 2 theoretical study with near explicit gas-phase chemistry

Carlton Xavier<sup>1</sup>, Anton Rusanen<sup>1</sup>, Putian Zhou<sup>1</sup>, Chen Dean<sup>1</sup>, Lukas Pichelstofer<sup>1</sup>, Pontus Roldin<sup>2</sup>, Michael Boy<sup>1</sup>

3 <sup>1</sup>Institute for Atmospheric and Earth Systems Research (INAR), Physics, University of Helsinki

4 <sup>2</sup>Division of Nuclear Physics, Lund University, Box 118, SE-22100, Lund, Sweden

5

6 **Correspondence** : Carlton Xavier ([carlton.xavier@helsinki.fi](mailto:carlton.xavier@helsinki.fi)), Michael Boy ([michael.boy@helsinki.fi](mailto:michael.boy@helsinki.fi))

7

## 8 **Abstract**

9 In this study we modeled secondary organic aerosols (SOA) mass loadings from the oxidation (by O<sub>3</sub>,  
10 OH and NO<sub>3</sub>) of five representative Biogenic Volatile Organic compounds (BVOCs): isoprene, endocyclic  
11 bond containing monoterpenes ( $\alpha$ -pinene and limonene), exocyclic double bond compound ( $\beta$ -pinene) and a  
12 sesquiterpene ( $\beta$ -caryophyllene). The simulations were designed to replicate idealized smog chamber and  
13 oxidative flow reactors (OFR). The master chemical mechanism (MCM) together with the peroxy radical  
14 autoxidation mechanism (PRAM), were used to simulate the gas-phase chemistry. The aim of this study was  
15 to compare the potency of MCM and MCM+PRAM in predicting SOA formation. SOA yields were in good  
16 agreement with experimental values for chamber simulations when MCM+PRAM was applied, while a  
17 standalone MCM under-predicted the SOA yields. Compared to experimental yields, the OFR simulations  
18 using MCM+PRAM over-predicted SOA mass yields for BVOCs oxidized by O<sub>3</sub> and OH, probably owing to  
19 increased seed particle surface area used in the OFR simulations. SOA yields increased with decreasing  
20 temperatures and NO concentrations and vice-versa. This highlights the limitations posed when using fixed  
21 SOA yields in a majority of global and regional models. Few compounds that play a crucial role (>95% of  
22 mass load) in contributing to SOA mass increase (using MCM+PRAM) are identified. The results further  
23 emphasized that incorporating PRAM in conjunction with MCM does improve SOA mass yields estimation.

24

## 25 1. **Introduction**

26 Atmospheric secondary organic aerosols, formed from gas to particle phase conversion of the  
27 oxidation products of volatile organic compounds (VOC) significantly impact the organic aerosol mass  
28 loadings (Griffin, 1999; Kanakidou et al., 2005). However, the scale of SOA contribution to the aerosol  
29 particle mass is still subjected to high uncertainties (Hao et al., 2011). The elevated aerosol particle



30 concentrations are shown to have inimical effects on health (Miller et al., 2007), and a varying degree of  
31 influence on the climate by forming cloud condensation nuclei (CCN), altering the cloud properties and  
32 radiative balance (Rosenfeld et al., 2014; Schmale et al., 2018). Therefore, it is acutely necessary to  
33 understand the role and contributions of SOA to the particle loading in the atmosphere. Biogenic VOCs from  
34 forest are estimated to contribute to about 90% of VOCs emissions globally (Guenther et al., 1995, 1999 and  
35 2000). The most important BVOCs for SOA formation are isoprene ( $C_5H_8$ ), monoterpenes ( $C_{10}H_{16}$ ) and  
36 sesquiterpenes ( $C_{15}H_{24}$ ). These compounds are all alkenes containing at least one carbon-carbon double bond,  
37 enabling them to undergo oxidation by the dominant atmospheric oxidants: the hydroxyl radical (OH), ozone  
38 ( $O_3$ ) and the nitrate radical ( $NO_3$ ). For some of the terpenes, initial oxidation steps can lead to formation of  
39 highly oxygenated organic molecules (HOM). These HOMs generally have low volatilities and can condense  
40 nearly irreversibly, thereby producing SOA (Ehn et al., 2014). HOMs, detected in both the ambient  
41 atmosphere and chamber experiments (Ehn M, et al., 2012) are formed by autoxidation (Berndt et al., 2016;  
42 Crouse and Nielsen, 2013) wherein peroxy radicals ( $RO_2$ ) undergo subsequent intramolecular H-shifts  
43 accompanied by rapid reactions with  $O_2$ . Autoxidation hence results in compounds containing multiple  
44 functional groups such as hydroxyls, peroxides and carbonyls (Bianchi et al., 2017, Bianchi et al., 2019).

45 A majority of chamber and flow-tube experiments have focused on HOM formation from the  
46 oxidation of various VOCs and their contribution to SOA mass loadings (Ehn et al., 2014; Kristensen et al.,  
47 2017). Oxidation of isoprene (Liu et al., 2016), endocyclic monoterpenes containing reactive double bonds  
48 such as  $\alpha$ -pinene and limonene (Zhao et al., 2015), or exocyclic double bond containing compounds such as  
49  $\beta$ -pinene (Jokinen et al., 2015) and sesquiterpenes such as  $\beta$ -caryophyllene (Chen et al., 2012) have been  
50 investigated. The SOA forming potential of various BVOCs depends on the isomeric structures (Friedman  
51 and Farmer, 2018; Keywood et al., 2004). Ozonolysis of compounds containing reactive endocyclic bonds  
52 such as  $\alpha$ -pinene produce higher SOA mass yields of 41% in comparison to those with exocyclic bonds ( $\beta$ -  
53 pinene), which produce mass yields of 17 % (Lee et al., 2006). One explanation for this dependence on the  
54 isomeric structure is attributed to the formation of HOMs (Ehn et al., 2014). Another important factor  
55 influencing HOM formation is the initial oxidant, as pointed out by Zhao and co-workers (2015). They  
56 showed that the SOA formation by OH oxidation of  $\alpha$ -pinene and limonene were lower when compared to  
57 their SOA formed by ozonolysis. Further they measured lower H/C ratio for SOA produced by monoterpene  
58 ozonolysis (experiments were carried out in dark with CO as OH scavenger), in comparison to OH oxidation  
59 of  $\alpha$ -pinene and limonene. This was attributed to the formation of  $RO_2$  radicals (monoterpenes +  $O_3$ ) which  
60 undergo internal hydrogen shifts and subsequently react with another  $RO_2$  radical, to form compounds  
61 containing carbonyl groups while losing hydrogen atoms in the process. A similar analysis was conducted by



62 Draper et al. (2015), who showed that an increase in NO<sub>2</sub> concentration reduced α-pinene ozonolysis SOA  
63 mass yields, while no appreciable reduction in mass yields are reported for β-pinene and Δ<sup>3</sup>-carene  
64 ozonolysis. On the other hand, the mass yields from limonene ozonolysis increased with increasing NO<sub>2</sub>  
65 concentrations (Draper et al., 2015). This disparity in mass yields for different BVOCs in the presence of NO<sub>2</sub>  
66 is possibly caused by the formation of high MW oligomers (or lack of in case of α-pinene) through oxidation  
67 with NO<sub>3</sub> that contribute to SOA mass loadings (Draper et al., 2015).

68 Due to computational limitations, many regional and canopy scale atmospheric chemistry models  
69 generally use isoprene and/or a representative monoterpene (generally α-pinene), to model SOA yields  
70 (Friedman and Farmer, 2018). The SOA yields of different monoterpenes vary with structure, NO<sub>x</sub> and  
71 temperature (Friedman and Farmer, 2018; Kristensen et al., 2017; Presto et al., 2005). This poses a limitation  
72 on using representative monoterpene fixed SOA yields in many of the global models and increases  
73 uncertainties in predicting cloud condensation nuclei concentrations, cloud droplet number concentrations and  
74 radiative balance due to aerosol loading's.

75 This work aims to investigate the SOA mass loading from the oxidation products of BVOCs with the  
76 atmospheric oxidants OH, O<sub>3</sub> and NO<sub>3</sub> with a specific focus on the BVOCs isoprene, α-pinene, β-pinene,  
77 limonene and β-caryophyllene. Further we study the effect of varying temperature (258.15 K – 313.15 K) and  
78 NO concentrations (0 - 5 ppb) on α-pinene oxidation mass yields. We use the master chemical mechanism  
79 (MCMv3.3.1) (Jenkin et al., 1997, 2012 and 2015; Saunders et al., 2003), a near explicit gas-phase chemical  
80 mechanism together with peroxy radical autoxidation mechanism (PRAM, Roldin et al., 2018) (PRAM +  
81 MCM). The aim is to understand the importance and contribution of peroxy radical autoxidation products to  
82 the SOA mass yields from terpenes.

83

## 84 2. Model description

### 85 2.1 Malte Box

86 MALTE (Model to predict new Aerosol formation in Lower TropospherE) is a one-dimensional  
87 model consisting of modules calculating boundary layer meteorology, emissions of BVOCs, gas-phase  
88 chemistry and aerosol dynamics with the aim to simulate particle distribution and growth in the lower  
89 troposphere (Boy et al., 2006). In this study, a zero-dimensional version, MALTE-Box is applied to simulate  
90 an ideal chamber and flow-tube environment (i.e. no wall losses effects are considered in this study). For the



91 simulations performed in this study the emission module was switched off while only employing the gas-  
92 phase chemistry and aerosol dynamics module.

93 Kinetic preprocessor (KPP) is used to generate a system of coupled differential equations to solve the  
94 gas-phase chemistry schemes (MCM+PRAM, Damian et al., 2002). The peroxy radical autoxidation  
95 mechanism (PRAM), (Roldin et al., 2018), formulated based on the oxidation of monoterpenes as described  
96 by Ehn et al. (2014) was incorporated alongside MCMv3.3.1. PRAM describes the evolution of peroxy  
97 radicals ( $RO_2$ ) from the ozonolysis of monoterpenes driven by subsequent H-shifts and  $O_2$  additions. The  
98 current version of PRAM considers HOM autoxidation for a fraction of the peroxy radicals formed during the  
99 ozonolysis of  $\alpha$ -pinene and limonene and OH oxidation of  $\alpha$ -pinene,  $\beta$ -pinene and limonene. PRAM considers  
100 temperature dependent autoxidation reaction rates, which is important when investigating the SOA mass  
101 yields at varying temperatures (Table 1c). It should be noted that the temperature dependence in PRAM is a  
102 first of its kind but needs further evaluation using recent measurements of HOM formation at different  
103 temperatures (e.g. Quéléver et al.2018).

104 The aerosol dynamics are simulated using the University of Helsinki Multicomponent Aerosol model  
105 (UHMA) originally from Korhonen et al. (2004). The model has undergone significant development since  
106 then to allow simulation with all the compounds from MCM. It now supports an unlimited number of  
107 condensing vapors and solves condensation using the analytical predictor of condensation method from  
108 Jacobson (1997). The condensation algorithm considers both, the Kelvin effect and Raoult's law. The  
109 processes included in the model are nucleation, condensation, evaporation, coagulation and deposition. The  
110 discretization of the size distribution and the time evolution is modeled with the moving section approach,  
111 with optional redistribution to a fixed grid. In this work, the redistribution is active to make the coagulation  
112 more accurate, since it requires that grid points are available near the size of the coagulated particles. In this  
113 study nucleation and deposition are not active, and hence are not considered. A total of 100 size bins ranging  
114 from 1nm to 20 $\mu$ m with the fixed grid was applied for this study.

115 A group contribution method based on Nannoolal et al. (2008) using the UManSysProp online system  
116 (Topping, 2016) was used to estimate the pure liquid saturation vapor pressures ( $p_0$ ) of the organic  
117 compounds in MCMv3.3.1. For the PRAM species,  $p_0$  were estimated using the functional group method  
118 SIMPOL (Pankow and Asher, 2008; see Roldin et al., 2018 for details)

## 119 2.2 Simulations

120 The simulations performed in this study are aimed to closely resemble an idealized smog chamber  
121 (batch mode setup) and an Oxidative Flow Reactor (OFR) without interactions between the gas phase and the



122 system walls. For the chamber runs, the VOC and oxidants were introduced at the beginning (time,  $t=0$  sec),  
123 set to certain concentrations and then allowed to react. Both chamber and OFR simulations are performed  
124 using ammonium sulfate seed particles which are introduced at time  $t=0$ . The condensation sink (CS) was  
125 inferred from the size distribution of seed particles used in the model. The CS for the chamber and OFR  
126 simulations was set to  $0.00067 \text{ s}^{-1}$  and  $0.067 \text{ s}^{-1}$  respectively. SOA mass yields obtained using an OFR are  
127 sensitive to short residence time used, hence the seed particle surface area should be chosen in order to  
128 overcome the mass yield underestimation (Ahlberg et al., 2019). CS sensitivity runs (Supplement Figure S1)  
129 were performed for  $\alpha$ -pinene- $\text{O}_3$  to determine the CS for which there are no appreciable change in mass yields  
130 with increasing particle surface.

131 The simulation for the chamber setup is run for a maximum time of 24 hours and ends when either of  
132 the 2 criteria are satisfied: (1) the simulation time reaches the 24-hour mark or (2) 90 % of the initial  
133 precursor VOC has reacted away. In the latter case the simulation is continued for an additional 2 hours to  
134 ensure enough time for the vapors to condense onto the seed particles. On the contrary, the OFR runs were  
135 simulated for a maximum residence time of 100 seconds, ensuring all initial precursor vapors were oxidized.  
136 Seed particles were also added in the OFR simulations. The oxidant concentrations used for the OFR  
137 simulations are significantly higher in comparison to the simulated chamber runs (~2 orders of magnitude  
138 larger). The time step for the chamber and flow-tube simulations are set to  $t=10 \text{ s}$  and  $t=0.1 \text{ s}$  respectively.  
139 The runs performed were oxidant specific (i.e. VOCs would be oxidized by only one specific oxidant at any  
140 given time). For the  $\text{O}_3$  specific simulations no OH could form in both, OFR and chamber setups, thus  
141 enabling oxidation of  $\text{O}_3$  to be the only pathway.

142 The simulations were performed at atmospheric relevant  $\text{NO}_x$  ( $\text{NO}_x = \text{NO} + \text{NO}_2$ ) concentrations,  
143 corresponding to  $[\text{NO}] = 0.5 \text{ ppb}$  and  $[\text{NO}_2] = 2.0 \text{ ppb}$  conditions with the relative humidity (RH) set to 60 %  
144 and temperature to 293.15 K. The RH value considered in this study is based on previous published  
145 experimental studies performed at ~60 % in both smog chamber (Bruns et al., 2015; Ehn et al., 2014;  
146 Stirnweis et al., 2017) and OFR (Ahlberg et al., 2019).  $\alpha$ -pinene ozonolysis runs were performed at four  
147 different temperatures: 258.15 K, 278.15 K, 303.15 K and 313.15 K, respectively. SOA mass yields are  
148 expected to increase with decreasing temperature (Saathoff and Naumann, 2009). A similar temperature  
149 dependence was observed by Kristensen et al. (2017) who observed SOA mass yield from  $\alpha$ -pinene  
150 ozonolysis at ~40 % and ~20 % at 258 K and 293 K respectively. Analogous to analyzing the effect of  
151 varying temperature on SOA yields, we study the variation in  $\alpha$ -pinene ozonolysis SOA mass yields by  
152 varying the  $\text{NO}_x$  concentrations. SOA yields for  $\alpha$ -pinene ozonolysis at high  $\text{NO}_x$  conditions should be  
153 suppressed (Ng and Chhabra, 2007), which could be due to the production of relatively, volatile organic



154 nitrates under high NO<sub>x</sub> conditions as compared to less volatile products during low NO<sub>x</sub> conditions (Presto et  
 155 al., 2005).

156 Furthermore, two different chemistry schemes were applied for the simulations. One scheme consisted  
 157 of only the MCM chemistry mechanism and the second included the MCM+PRAM chemistry mechanism.  
 158 Table 1a shows the concentrations of different BVOCs and Table 1b shows the oxidants concentrations used  
 159 for the simulations.

160 **Table 1a.** Concentrations of different BVOCs

<b>α-pinene (ppb)</b>	<b>β-pinene (ppb)</b>	<b>Isoprene (ppb)</b>	<b>Limonene (ppb)</b>	<b>β-caryophyllene (ppb)</b>
0.5, 1.0, 5.0, 50.0, 100.0, 200.0	0.5, 1.0, 5.0, 50.0, 100.0, 200.0	5.0, 50.0, 100.0, 200.0	1.0, 5.0, 50.0, 100.0, 200.0	0.5, 1.0, 2.0, 5.0, 10.0

161

162 **Table 1b.** Concentrations of different oxidants for chamber and flow-tube runs

<b>OH (* 10<sup>6</sup> #/cm<sup>3</sup>) - chamber</b> <b>OH (* 10<sup>8</sup> #/cm<sup>3</sup>) - OFR</b>	<b>O<sub>3</sub> (* 10<sup>11</sup> #/cm<sup>3</sup>) - chamber</b> <b>O<sub>3</sub> (* 10<sup>13</sup> #/cm<sup>3</sup>) - OFR</b>	<b>NO<sub>3</sub> (* 10<sup>7</sup> #/cm<sup>3</sup>) - chamber</b> <b>NO<sub>3</sub> (* 10<sup>9</sup> #/cm<sup>3</sup>) - OFR</b>
2.0, 5.0, 10.0, 50.0, 100.0	1.0, 5.0, 10.0, 50.0, 100.0	1.0, 5.0, 10.0, 50.0, 100.0

163

164 **Table 1c.** NO concentrations and temperatures used for α-pinene ozonolysis

<b>NO (ppb)</b>	0.5 (default), 0, 0.2, 1, 2, 5
<b>Temperature (K)</b>	293.15 (default), 258.15, 278.15, 303.15, 313.15

165

### 166 2.3 Mass Yields

167 The SOA mass yields (Y) are determined by calculating the ratio of the amount of SOA or mass  
 168 concentration of organic aerosol formed (C<sub>OA</sub>) to the amount of VOC (ΔVOC) reacted:

169

$$Y = \frac{C_{OA}}{\Delta VOC} \quad (1)$$



170 A volatility basis set is fit to the data to obtain the volatility distribution. In this study equilibrium  
171 partitioning was only assumed for deriving the volatility distribution based on the model simulations.  
172 Following Donahue et al. (2006), the SOA is assumed to be in equilibrium with the gas-phase and using the  
173 effective saturation concentration  $C_i^*$  spaced logarithmically. The individual product partitioning to the  
174 particle phase can be estimated using

$$175 \quad E_i = \left( 1 + \frac{C_i^*}{C_{OA}} \right)^{-1} \quad (2)$$

176 Where  $E_i$  is the fraction of species in the condensed particle phase. The above equation determines the  
177 fraction of species in the particle phase as well as in the gas phase. For example, if we assume  $C_{OA} = 10 \mu\text{g m}^{-3}$   
178 a species with  $C^* = 10 \mu\text{g m}^{-3}$  will partition 50 % to condensed phase and the rest 50% will reside in the gas  
179 phase. The fidelity of this equilibrium partitioning enables the parameterization of product vapors in volatility  
180  $C^*$  bins that are near the  $C_{OA}$  concentrations (Henry et al., 2012).

181

### 182 3. Results and Discussion

#### 183 3.1 BVOCs – O<sub>3</sub> chamber and flow-tube simulations

184 SOA mass yields were simulated for the oxidation of various biogenic volatile organic compounds  
185 (isoprene,  $\alpha$ -pinene, limonene and  $\beta$ -caryophyllene,  $\beta$ -pinene) by dominant atmospheric oxidants OH, O<sub>3</sub> and  
186 NO<sub>3</sub>. The following section examines the comparison between the yields derived using MCM+PRAM and a  
187 standalone MCM for chamber and flow-tube experiments. In Fig 1. the upper panel indicates MCM+PRAM  
188 contribution to SOA mass from BVOCs ozonolysis and the lower panel shows the differences between the  
189 yields obtained from the MCM+PRAM ( $Y_{\text{MCM+PRAM}}$ ) and MCM scheme ( $Y_{\text{MCM+PRAM}} - Y_{\text{MCM}}$ ).

190 The abscissa, depicted on a log scale, considers the entire range of SOA mass loadings from 1-1150  
191  $\mu\text{g/m}^{-3}$ . Each data point is representative of simulated SOA mass yields resulting from variable BVOC  
192 loading. The resulting mass yields for  $\alpha$ -pinene in the range shown in Table 2a are consistent with the yields  
193 found in various smog chamber experiments. Kristensen et al. (2017) found mass yields of 0.22 and 0.21 for  
194  $\alpha$ -pinene ozonolysis at 293 K with SOA mass loadings of 62 and 59  $\mu\text{g m}^{-3}$ , respectively, while Pathak et al.  
195 (2007) found similar mass yields values in the range of 0.16 – 0.21 for mass loadings between 33.7 – 50.7  $\mu\text{g}$   
196  $\text{m}^{-3}$ . These values are within the range of mass yields derived using MCM+PRAM (0.15 - 0.2) while those  
197 derived with only MCM severely under-predict the mass yields. The MCM+PRAM also shows better  
198 agreement with experiments when estimating the lower range mass yields for SOA mass loadings of < 15  $\mu\text{g}$





199  $\text{m}^{-3}$ . This is supported by the values obtained by Shilling et al. (2008), where the authors measured a 0.09  
200 yield from  $\alpha$ -pinene ozonolysis for SOA mass loading of  $10.6 \mu\text{g m}^{-3}$ . Limonene ozonolysis mass yields using  
201 MCM+PRAM in comparison to standalone MCM, are much closer to the values given by Waring (2016),  
202 wherein he measured high yields of 0.26 - 1.06 for SOA loadings of 1.7 -  $718.4 \mu\text{g m}^{-3}$ .

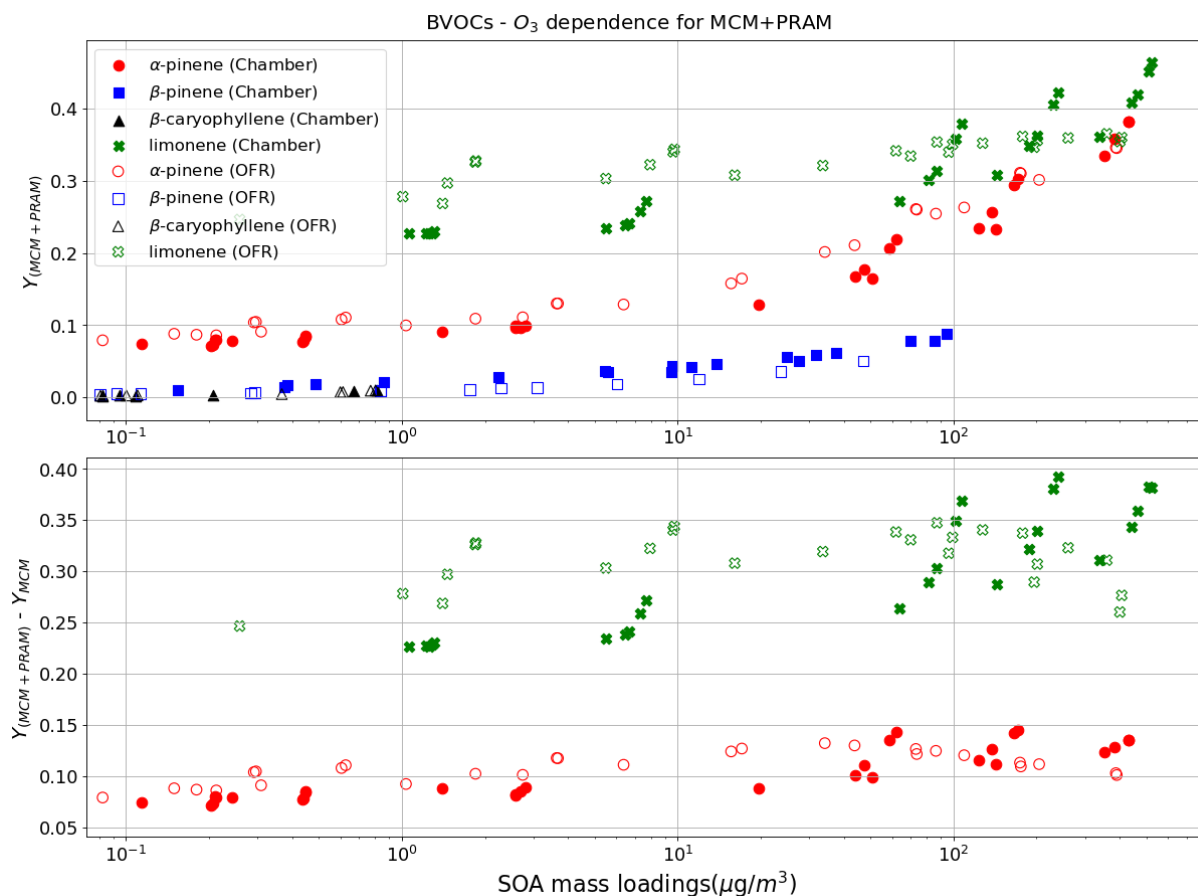
203 The formation of HOM from  $\beta$ -pinene ozonolysis is low (Ehn et al., 2014; Jokinen et al., 2015) and  
204 hence not considered in PRAM. The peroxy radical autoxidation mechanism for  $\beta$ -caryophyllene ozonolysis  
205 has not yet been developed and hence is not considered in PRAM. Chen et al. (2012) measured SOA particle  
206 mass yield for  $\beta$ -caryophyllene ozonolysis in the range of 0.1- 0.2 for mass loadings  $M_{\text{org}} < 10 \mu\text{g m}^{-3}$  and  
207 ascertained the  $\text{O}_3$  concentration insensitivity to the yields. Pathak et al. (2008) measured the  $\beta$ -pinene  
208 ozonolysis mass yields in the range of 0.013- 0.081 for lower reacted concentrations (8-40 ppb) of  $\beta$ -pinene,  
209 while Griffin (1999) measured a yield from 0.01-0.17 for reacted  $\beta$ -pinene in the range of 30 -180 ppb. When  
210 comparing the measured mass yield values for  $\beta$ -caryophyllene and  $\beta$ -pinene ozonolysis to the modeled  
211 values using the MCM scheme, it is evident that the MCM scheme drastically under-predicts the SOA mass  
212 yields.

213 Today oxidation flow reactor (OFR) experiments are complementing the traditional batch mode smog  
214 chamber experiments. The OFR generally exhibits lower mass yields compared to the smog chamber  
215 experiments at ranges of equivalent oxidant exposure (Lambe et al., 2015). We modeled flow-tube simulation  
216 after the potential aerosol mass (PAM) OFR, where the residence time is in the order of a few to several  
217 minutes (Lambe et al., 2011). Our model simulations are performed with a maximum residence time of 100  
218 seconds with  $\text{O}_3$  exposures ranging from  $1.0 \times 10^{15} - 1.0 \times 10^{17} \text{ molecules cm}^{-3} \text{ s}$  (residence time  $\times [\text{O}_3]$ ).  
219 Kang and Root (2007) measured a value of 0.2 for ozonolysis of  $\alpha$ -pinene for an initial precursor VOC  
220 concentration of 100 ppbv, while we obtain 0.25-0.3 for the similar initial precursor concentrations. The OFR  
221 yields for  $\beta$ -pinene are significantly lower (0.02) than the values measured by Kang and Root (2007) wherein  
222 they measured a yield of 0.49 for similar initial precursor concentrations. Addition of seed particles promotes  
223 condensation, leading to increased SOA yields (Lambe et al., 2015) which was confirmed by Ahlberg et al,  
224 (2019). Kang and Root (2007) found that using seed particles, the yield from  $\alpha$ -pinene ozonolysis increased  
225 by a factor of  $\sim 1.4$  which can explain our yields for  $\alpha$ -pinene ozonolysis simulations, while the absence of a  
226 PRAM for  $\beta$ -pinene could explain the low values from our simulation. The mass spectra plot (Figure S2)  
227 shows that PRAM contributes the majority of dimers to the particle phase, while MCM dominate monomer  
228 contribution. Another interesting facet of Figure S2 are the different condensing compounds in both OFR and  
229 chamber simulations. The higher absolute  $\text{RO}_2$  concentrations in the OFR simulations explain the lower  
230 concentration of HOM monomers and dimers relative to the chamber simulations, i.e. the high  $\text{RO}_2$





231 concentrations in the OFR cause termination of the peroxy radical autoxidation chain before the RO<sub>2</sub> become  
 232 highly oxygenated, thereby influencing SOA yields. Hence, this should be taken into account when using  
 233 yields from OFR as inputs to regional and global models.



234 **Figure 1.** The mass yields from the ozonolysis of BVOCs modelled after chamber and flow-tube settings. The figure shows a  
 235 comparison of SOA mass yields obtained from simulations with MCM + PRAM and PRAM. The BVOCs are represented by  $\alpha$ -  
 236 pinene (red circles),  $\beta$ -pinene (blue squares), limonene (green stars) and  $\beta$ -caryophyllene (black triangles) with the filled and open  
 237 symbols depicting the chamber and oxidation flow reactor (OFR) simulations respectively.

**Table 2.** Mass yields for BVOCs ozonolysis at 293 K for different range of mass loadings using a chamber<sup>†</sup>  
 and OFR<sup>||</sup> setup.

SOA mass loading ( $\mu\text{g m}^{-3}$ )	MCM + PRAM mass yields range	MCM mass yields range	BVOC	Experimental yields	References



0 - 15 <sup>†</sup>	0.07– 0 .08	0.00 – 0.06	α-pinene	0.09 (10.6)	Shilling et al. (2008)
16 - 60 <sup>†</sup>	0.12 – 0.20	0.06 – 0.11	α-pinene	0.16 - 0.21	Pathak et al. (2007)
61 – 200 <sup>†</sup>	0.22 – 0.30	0.12 – 0.15	α-pinene	0.22 (62)	Kristensen et al. (2017)
1.1– 550 <sup>†</sup>	0.24 -0.48	0.007-0.06	limonene	0.26-1.06	Waring (2016)
0-100 <sup>  </sup>	0.07-0.25	0-0.13	α-pinene	0.2	Kang and Root (2007)

238

### 239 3.2 BVOCs – OH chamber and flow-tube simulations

240 The  $\Delta Y$  in the lower panel of Figure 2 for limonene,  $\beta$ -pinene and  $\alpha$ -pinene resulting from the fact that  
241 PRAM considers peroxy radical autoxidation product formation from OH oxidation of these BVOC's. The  
242 results for SOA mass yields of OH oxidation of  $\alpha$ -pinene using MCM+PRAM is close to the measured values  
243 (Kristensen et al., 2017), while using only MCM under-predicts the mass yields. Similarly, the current lack of  
244 peroxy radical autoxidation product mechanism for  $\beta$ -caryophyllene and isoprene result in  $\Delta Y = 0$  values for  
245 PRAM. The maximum SOA mass yield for OH oxidation of  $\alpha$ -pinene is lower than the yield from ozonolysis  
246 which is suspected to arise due to the formation of more volatile oxidation products produced during OH  
247 oxidation (Bonn and Moortgat, 2002; Kristensen et al., 2014). For  $\beta$ -caryophyllene, Griffin (1999) measured  
248 SOA mass yields in the range of 0.37 – 0.79 for mass loadings of 17 - 82  $\mu\text{g m}^{-3}$  while Tasoglou and Pandis  
249 (2015) measured yields around 0.2 for photo-oxidation at low  $\text{NO}_x$  conditions for loadings of 10  $\mu\text{g m}^{-3}$ .  
250 These values are in good agreement with our results which show a similar yield range of 0.3 – 0.7 for  
251 loadings between 20 - 100  $\mu\text{g m}^{-3}$  and 0.21 for loading of 10  $\mu\text{g m}^{-3}$ . Currently there are no experiments  
252 providing HOM yields from experiments of OH oxidation of  $\beta$ -caryophyllene, and hence, not included in  
253 PRAM. The simulation results for yields from OH oxidation of  $\beta$ -caryophyllene, indicate that the MCM  
254 scheme is able to reproduce the experimental values. The mass yields derived from OH oxidation of isoprene  
255 vary from 0.01 - 0.31 covering a range of mass loadings from 0.003 - 132  $\mu\text{g m}^{-3}$ . At low mass loadings < 10  
256  $\mu\text{g m}^{-3}$  the maximum yield obtained is  $\sim 0.06$ , which is a factor of 2 greater than the experimental results  
257 obtained by Lee et al. (2006) and Kroll et al. (2005), where they measured yields of 0.02 and 0.01 – 0.03  
258 respectively. Liu et al. (2016) measured higher mass yields ( $> 0.1$ ) for similar loadings with a maximum  
259 upper limit yield of 0.15 for 22  $\mu\text{g m}^{-3}$ , while our results under-predict the yields ( $\sim 0.10$ ) for similar  
260 loadings. The OH oxidation of  $\beta$ -pinene and limonene results in a maximum yield of 0.28 for high mass  
261 loading of 319  $\mu\text{g m}^{-3}$  and 0.56 for loadings of 630  $\mu\text{g m}^{-3}$  respectively. These values are similar to the

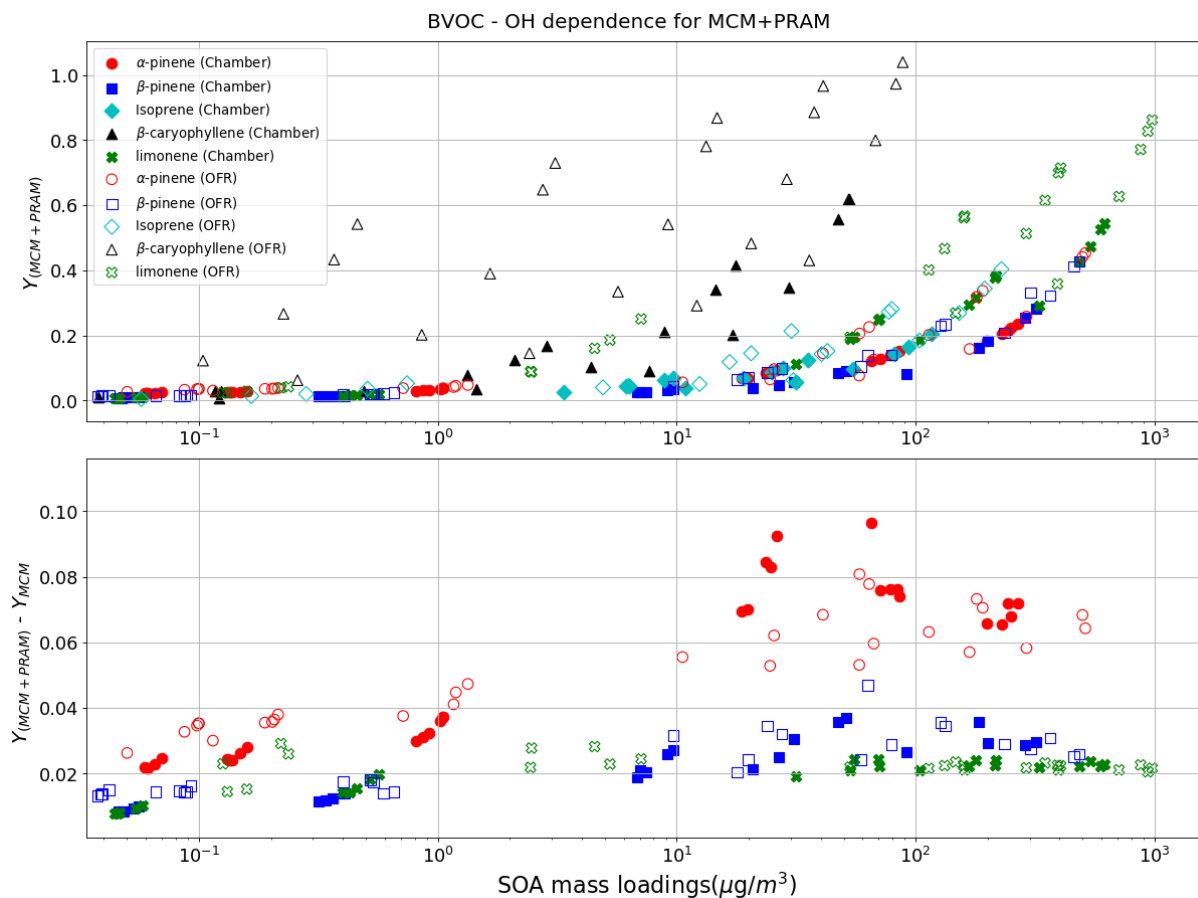


262 measurements obtained by Lee et al. (2006) wherein they measured a yield of 0.31 for  $\beta$ -pinene SOA mass  
263 loadings of  $293 \mu\text{g m}^{-3}$  and 0.58 for limonene SOA mass loadings of  $394 \mu\text{g m}^{-3}$ . Yields for limonene SOA  
264 mass loadings of  $350 \mu\text{g m}^{-3}$  are around 0.31 which is lower than the experimental values, measured by Lee et  
265 al. (2006). The  $\beta$ -pinene SOA yields are comparatively well represented by MCM+PRAM in comparison to  
266 the standalone MCM. On the other hand, the limonene mass yields are under-predicted by MCM+PRAM.

267 The OFR simulations results for the OH oxidation of BVOCs with an equivalent exposure range from  
268  $2.0 \times 10^{10} - 2.0 \times 10^{12}$  molecules  $\text{cm}^{-3} \text{s}$ , is shown in Fig. 2. Friedman and Farmer (2018) found mass yields  
269 of  $7 \times 10^{-4} - 0.086$  for  $\alpha$ -pinene (ammonium sulfate seeded experiment), 0 - 0.12 for  $\beta$ -pinene (no seed  
270 particles) and 0.0017 - 0.026 for limonene (no seed particles), by varying the OH exposures between  $4.7 \times$   
271  $10^{10} - 7.4 \times 10^{11}$  molecules  $\text{cm}^{-3} \text{s}$ . Our simulated yields for OH oxidation of  $\alpha$ -pinene ( $\sim 0.05 - 0.31$ ),  $\beta$ -  
272 pinene ( $\sim 0.019 - 0.2$ ) and limonene suggest higher mass yields at both measured lower and higher values of  
273 values of OH exposures and monoterpene concentrations ( $\sim 12 - 270$  ppb). In contrast to the experiments,  
274 every simulation contained higher particle surface area, which could explain the higher simulated mass yields  
275 for the compounds.

**Table 3.** Mass yields for OH oxidation of BVOCs at 293 K for different range of mass loadings using a chamber<sup>†</sup> and OFR<sup>||</sup> setup.

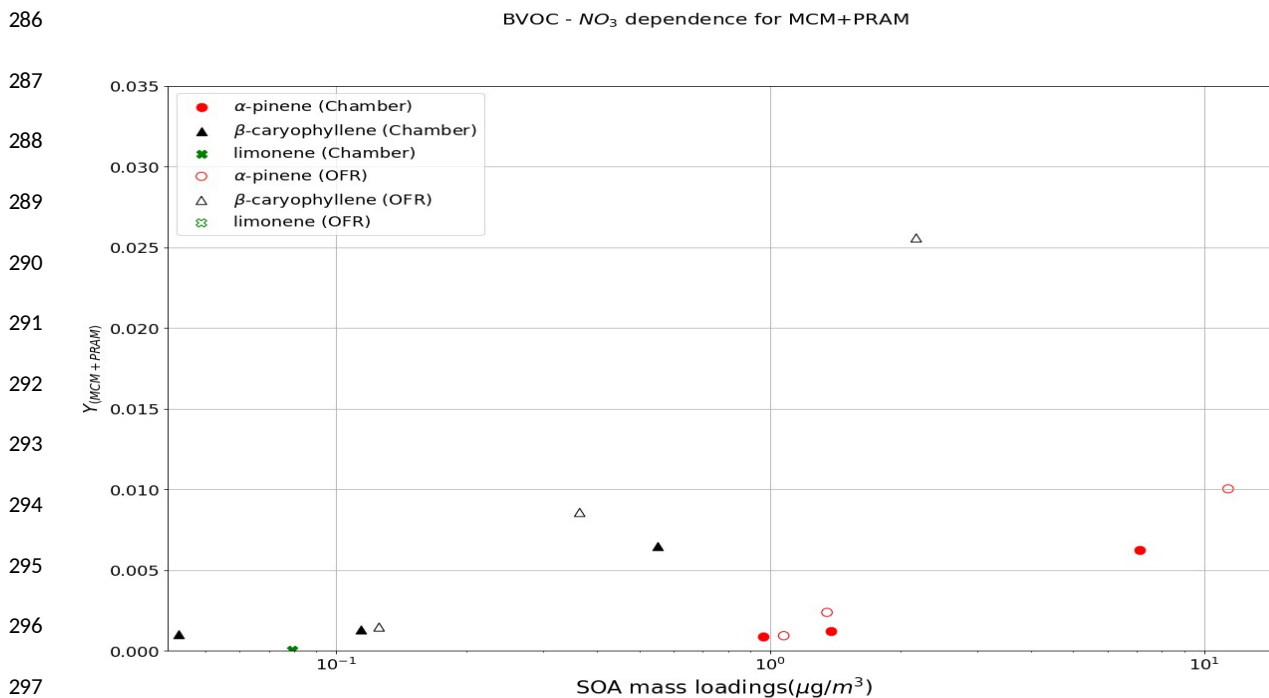
SOA mass loading ( $\mu\text{g m}^{-3}$ )	MCM + PRAM mass yields	MCM mass yields	BVOC	Experimental yields	References
320 <sup>†</sup>	0.28	0.25	$\beta$ -pinene	0.31	Lee et al. (2006)
350 <sup>†</sup>	0.31	0.06 – 0.11	limonene	0.58	Lee et al. (2006)
0-300 <sup>  </sup>	0.05 – 0.31	0. – 0.2	$\alpha$ -pinene	$7 \times 10^{-4} - 0.086$	Friedman and Farmer (2018)
0-300 <sup>  </sup>	0.019-0.2	0-0.13	$\beta$ -pinene	0 - 0.12	Friedman and Farmer (2018)



276 **Figure 2.** The mass yields from OH oxidation of BVOCs modeled after chamber and flow-tube settings. The figure shows a  
277 comparison of SOA mass yields obtained from application of MCM+PRAM and only MCM. The color scheme is the same as in  
278 figure 1. Additionally, isoprene has been included as it reacts with OH and produces considerable SOA yields.

### 279 **BVOC – NO<sub>3</sub> chamber and OFR simulations**

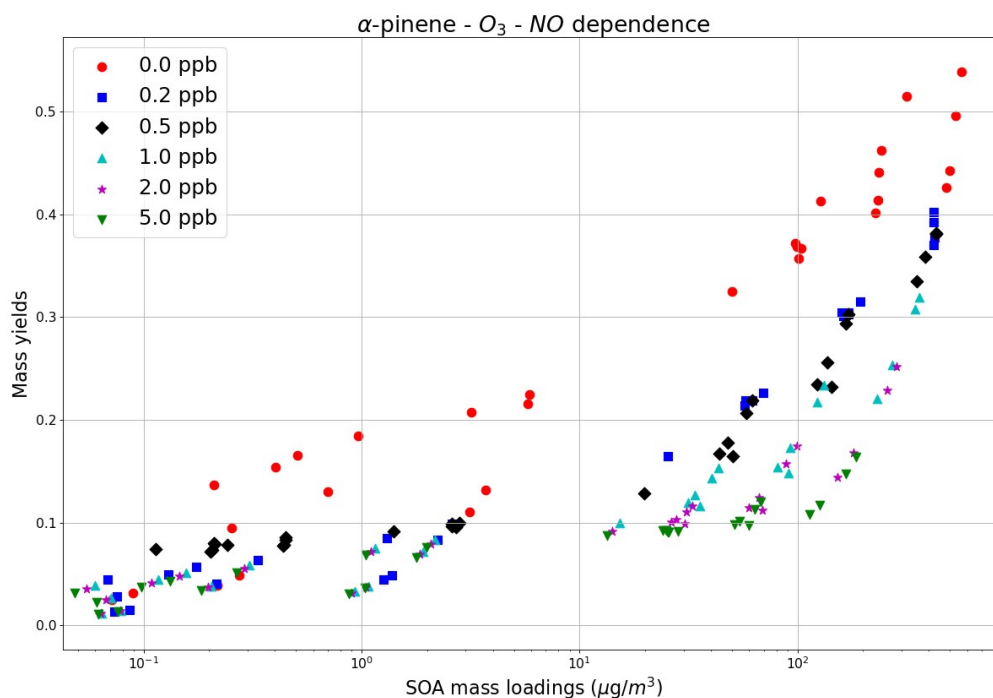
280 The yields obtained for oxidation of  $\alpha$ -pinene (0.002-0.007) by NO<sub>3</sub> are low in comparison to those  
281 obtained by Nah et al. (2016), where they measured a yield of 0.036. Measured mass yields for limonene  
282 oxidation by NO<sub>3</sub> resulting in mass yields between 0.25-0.4 (Fry et al., 2011), whereas we obtain negligible  
283 (~0.0003) mass yields for the same. Due to limited experimental constraints, PRAM presently does not  
284 consider autoxidation of RO<sub>2</sub> formed from NO<sub>3</sub> oxidation of VOCs, which could explain the huge discrepancy  
285 between the measured and simulated mass yields.



298 **Figure 3.** The mass yields from NO<sub>3</sub> oxidation of BVOCs modeled after chamber and flow-tube settings. The figure shows a  
299 comparison of SOA mass yields obtained from application of MCM+PRAM. Appreciable mass yields were only obtained for  $\alpha$ -  
300 pinene, limonene and  $\beta$ -caryophyllene.

### 301 3.3 NO<sub>x</sub> dependence

302 Organic oxidation mechanisms are sensitive to NO<sub>x</sub> concentrations as they change the fate to RO<sub>2</sub>  
303 radical formed, thereby impacting the distribution of reaction products and aerosol formation (Presto et al.,  
304 2005; Zhao et al., 2018). We modeled the SOA mass yields for  $\alpha$ -pinene - O<sub>3</sub> setup with varying NO<sub>x</sub>  
305 concentrations (NO was varied whereas NO<sub>2</sub> was kept constant for all the runs), for initial  $\alpha$ -pinene mixing  
306 ratios in the range 0.5 - 200 ppb (Fig. 4). A maximum SOA yield value of 0.55 is obtained for a combination  
307 of the lowest value of NO (0 ppb, red circles). As the NO concentrations increase from 0.2 ppb (blue squares)  
308 to 5 ppb (green inverted triangles) the yields begin to decrease, and this pattern is observable and valid for all  
309 concentration ranges of reacted precursor VOC. The NO<sub>x</sub> dependence of  $\alpha$ -pinene ozonolysis is consistent  
310 with the findings of Draper et al. (2015) and Presto et al. (2005) wherein they observed a trend of decreasing  
311 SOA mass yields for  $\alpha$ -pinene ozonolysis with increasing NO<sub>x</sub> concentrations. NO<sub>x</sub> concentrations alter the  
312 HO<sub>2</sub>/RO<sub>2</sub> ratio thereby impacting competing peroxy radical (RO<sub>2</sub>) reaction pathways (Presto et al., 2005;  
313 Sarrafzadeh et al., 2016).



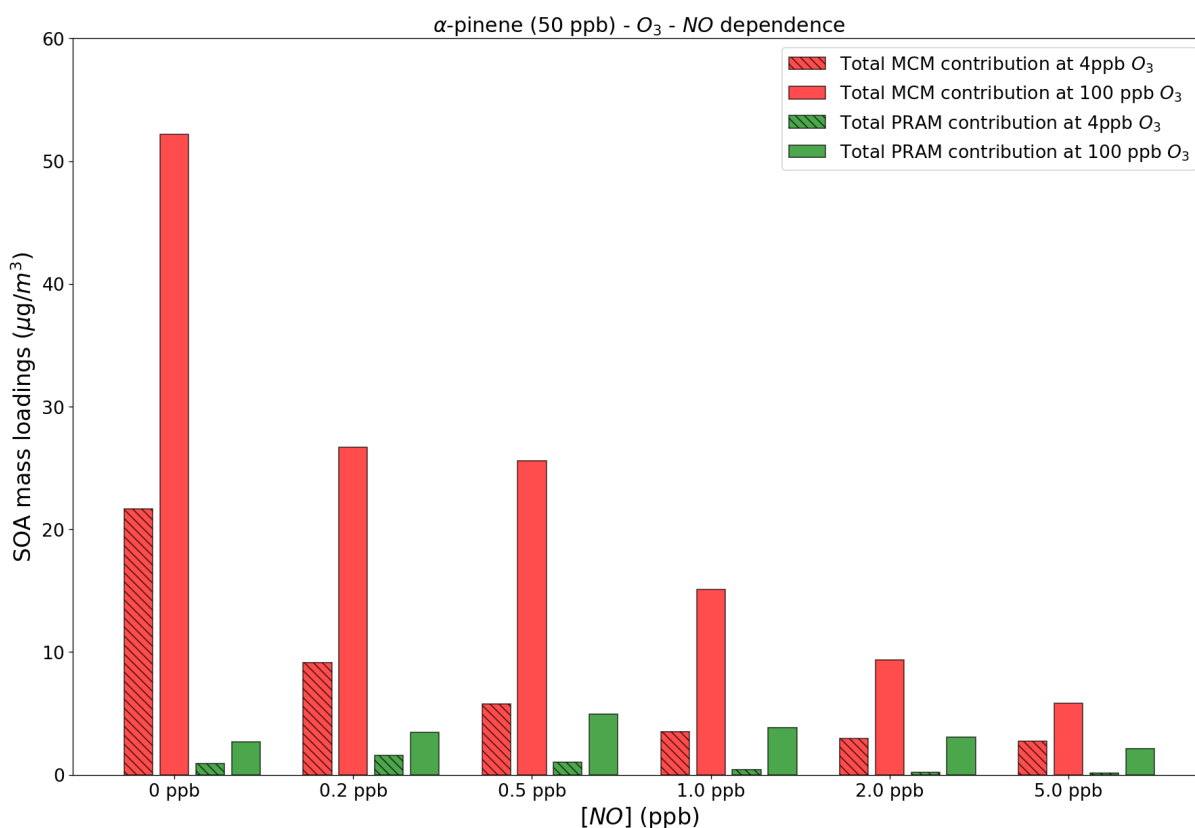
314 **Figure 4.** The SOA mass yields from  $O_3$  oxidation of  $\alpha$ -pinene modeled for different  $NO$  concentrations with the chamber setup.  
315 The model runs were performed using MCM+PRAM.

316 At low  $NO_x$  concentrations  $RO_2$  radicals undergo rapid autoxidation until they react with  $HO_2$  or  $RO_2$   
317 resulting in production of low volatility hydro-peroxide products (Sarrafzadeh et al., 2016), closed shell  
318 monomers or dimers (Ehn et al., 2011; Roldin et al., 2018), which increase SOA mass. This contrasts with high  
319  $NO_x$  conditions where the  $RO_2+NO$  reactions dominate over reactions with  $HO_2$  or  $RO_2$ , resulting in the  
320 formation of more volatile products such as aldehydes, ketones and organonitrates (Presto et al., 2005;  
321 Sarrafzadeh et al., 2016), and likely suppressing the autoxidation process leading to a decrease in SOA mass  
322 loadings (Ehn et al., 2014).

323 Figure 5 shows the absolute contributions to SOA mass loadings by PRAM and MCM compounds at  
324 two different  $O_3$  concentrations of 4 and 100 ppb and varying  $NO$  concentrations. The figure shows that with  
325 an increase in  $NO$  concentrations the contribution of PRAM compounds to the particle phase decreases at  
326 both 4 and 100 ppb of  $O_3$  concentrations. In PRAM the  $RO_2 + NO$  reaction leads either to the formation of  
327 organonitrate HOM, closed shell monomers with carbonyl group or fragmentation products with higher  
328 volatility (Roldin et al., 2018). HOM Dimer formation is suppressed with increasing  $NO$  concentrations in



329 PRAM (Roldin et al., 2018) which explains the lower contribution by PRAM compounds to SOA mass  
330 loadings with increasing NO. The PRAM contribution increases at low NO (<1 ppb) and then decreases  
331 thereafter. At low NO concentrations (<1ppb), first generation RO<sub>2</sub> are capable of undergoing autoxidation  
332 forming highly oxygenated RO<sub>2</sub> which subsequently reacts with NO forming organic nitrates (Ehn et al.,  
333 2014). As NO concentrations exceed 1ppb the first generation RO<sub>2</sub> is scavenged by NO thereby reducing the  
334 concentration of organonitrate HOM (Ehn et al., 2014), possibly affecting SOA yields. The MCM  
335 contribution also decreases with increasing NO concentrations mostly due to the formation more volatile  
336 organonitrates (Jenkin et al., 2019).



337 **Figure 5.** Contribution to the SOA mass loadings by total PRAM and MCM compounds at different NO<sub>x</sub> levels and O<sub>3</sub>  
338 concentrations. For comparison we use 4 ppb and 100 ppb O<sub>3</sub> concentrations, respectively, at 50 ppb  $\alpha$ -pinene.

### 339 3.4 Temperature dependence

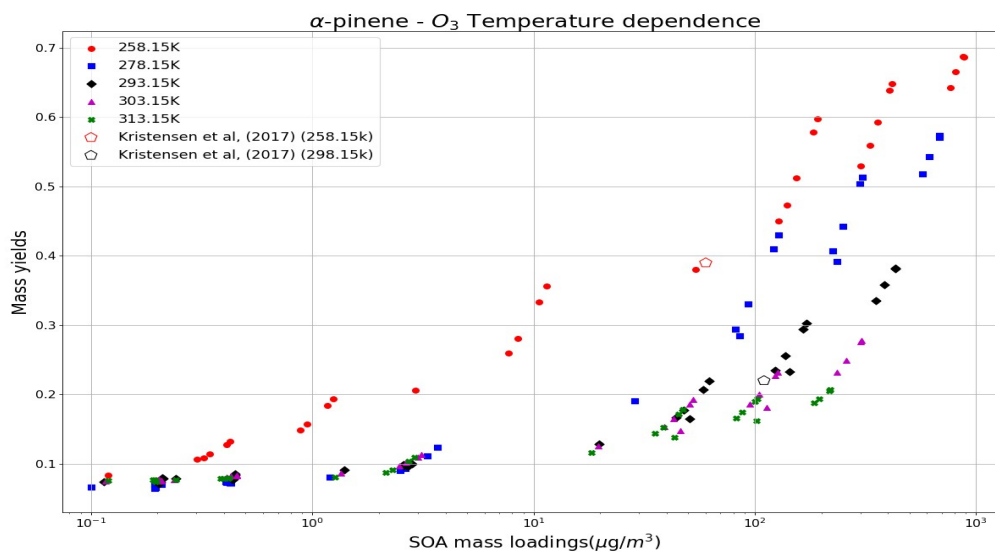
340 The formation of SOA from  $\alpha$ -pinene ozonolysis in the temperature range of 258.15 - 313.15 K was  
341 investigated in this study using MCM+PRAM. Strong dependence of SOA mass yield on temperature was  
342 reported by Saathoff and Naumann, (2009) wherein they measured the decreasing mass yields from 0.42 at





343 273.15 K to 0.09 to 313.15 K for SOA loadings of 53 and 92  $\mu\text{g m}^{-3}$  respectively. Our results in Figure 6  
344 show increasing SOA mass yields for  $\alpha$ -pinene ozonolysis with decreasing temperature, which is attributed to  
345 the augmented condensation of oxidation products termed as semi volatile organic compounds (SVOC)  
346 (Kristensen et al., 2017) at lower temperatures.

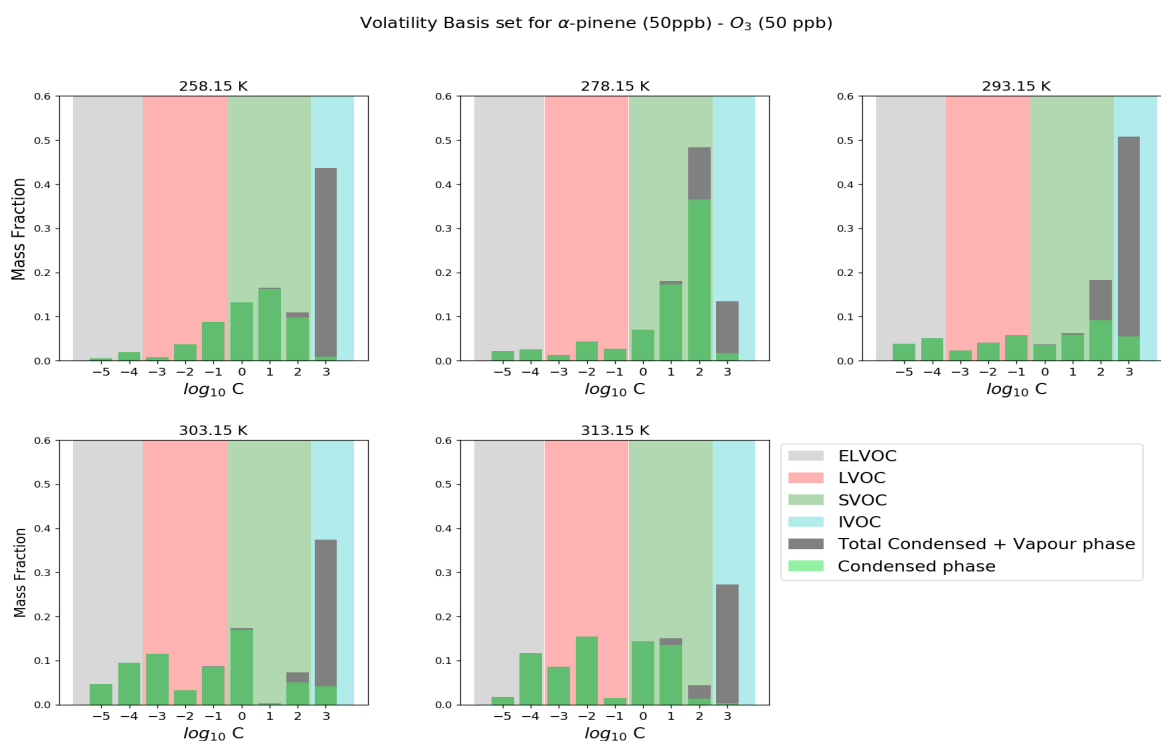
347 For  $\alpha$ -pinene maximum mass loading  $< 150 \mu\text{g m}^{-3}$  the mass yields reach a maximum value of 0.38 at  
348 temperatures as low as 258.15 K and decreases to 0.27 for a temperature of 293.15 K to 0.1 for the  
349 temperature of 313.15 K. These yields are comparable to the results obtained by Kristensen et al.  
350 (2017) where they measured yields of 0.39 for 258.15 K and 0.22 for 293.15 K for mass loading  $< 150 \mu\text{g m}^{-3}$ .  
351 The results show a weak dependence of SOA mass yields on temperatures in the range of 278.15 K - 313.15  
352 K at low SOA mass loadings but become more pronounced as the mass loadings increase. At the lowest  
353 temperature of 258.15 K the mass yields are higher in comparison to other temperatures regardless the mass  
354 loadings. These results are in good agreement with the findings by Pathak et al. (2007) where they found a  
355 strong temperature dependence of SOA mass yields at lower temperature (0 – 15° C), which decreases as the  
356 temperature increases. Furthermore, similar to the measurements made by Pathak et al. (2007), our  
357 simulations were able to reproduce the experimental findings that show no appreciable differences in the SOA  
358 mass yields for loadings below 1  $\mu\text{g m}^{-3}$  (initial mixing ratio of 1 ppb) for temperatures  $> 273.15$  K.



359 **Figure 6.** Temperature dependence of SOA mass yields at different temperatures using the MCM+PRAM. The open pentagons  
360 represent measurement data from Kristensen et al. (2017) at 258.15 K and 298.15 K.



361 Figure 7 shows the volatility distribution of  $\alpha$ -pinene ozonolysis derived SOA at different  
362 temperatures. The saturation vapor pressure limits for defining extremely low volatility (ELVOCs - grey  
363 shaded), low volatility (LVOCs - red shaded), semi volatile (SVOCs - green shaded) and intermediate  
364 volatility (IVOCs - cyan shaded) organic compounds used in the Volatility basis set (VBS) are set according  
365 to the values suggested in Donahue et al. (2012). In this work, we categorize compounds (ELVOCs, LVOCs,  
366 SVOCs and IVOCs) based on effective saturation vapor pressures ( $C^*$ ) in the range of  $\{10^{-5}$  to  $10^3\}$   $\mu\text{g m}^{-3}$   
367 and temperature of 298 K (Donahue et al., 2009). At the lowest temperature of 258.15 K, the SVOCs  
368 contribution to the particle phase is dominant in comparison to LVOCs and ELVOCs, a trend which is  
369 subsequently reversed as the temperatures are increased. At 293.15 K a majority of SVOCs and IVOCs are in  
370 the gas phase while the contribution of LVOCs and ELVOCs to particle phases increases. These results are in  
371 good agreement with observations made by Kristensen et al. (2017) wherein they observed an increasing  
372 contribution of SVOCs at sub-zero temperatures of 258.15 K, which decrease the fraction of SOA formed  
373 from ELVOCs. Again, it should be noted that the temperature dependence of peroxy radical autoxidation  
374 product formation still needs further validation based on recent experiments (e.g. Quéléver et al., 2018).  
375

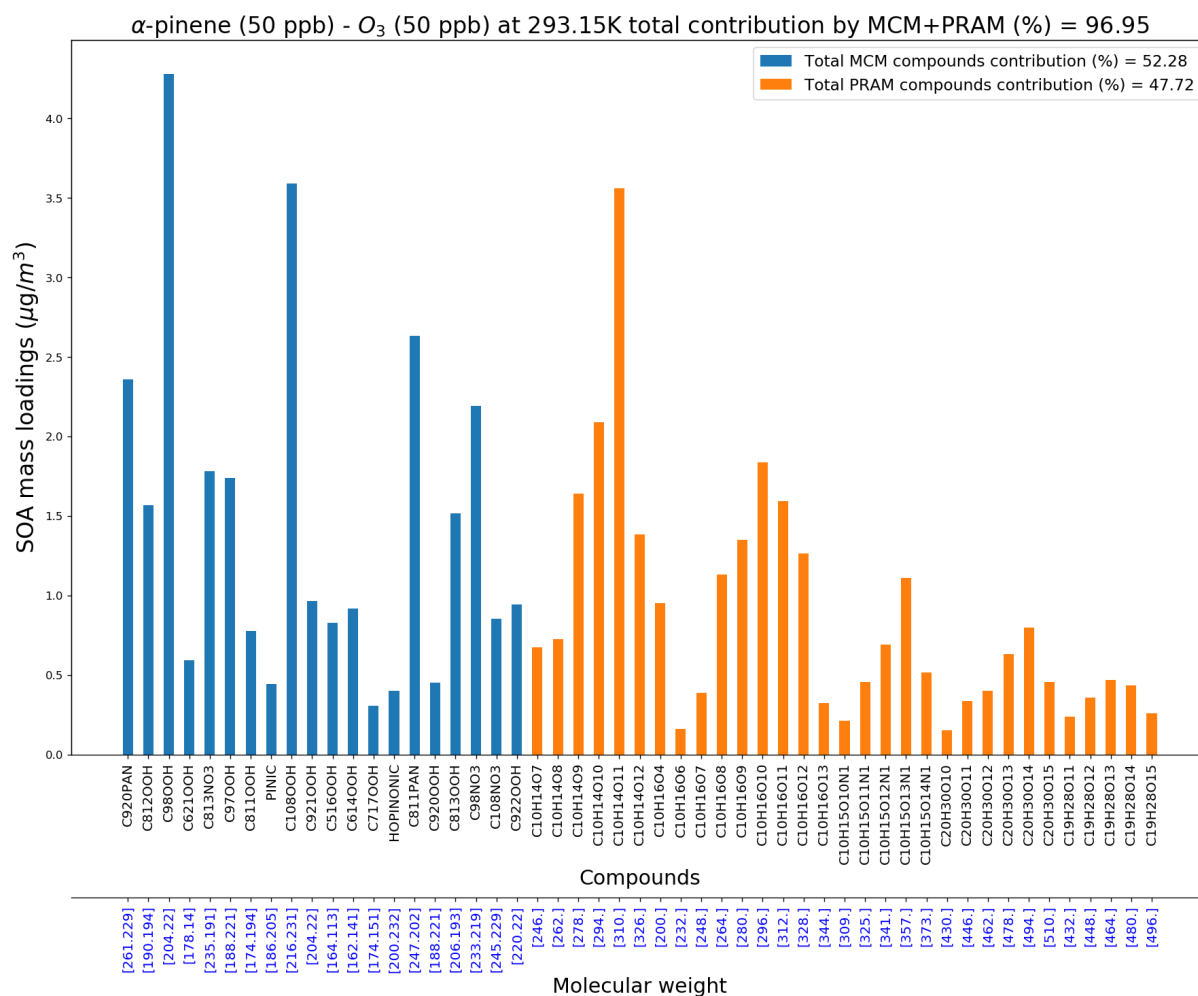


376 **Figure 7.** Modeled volatility distribution of SOA at different temperatures. The volatility bins span a range of effective saturation  
377 vapor pressures  $C = C^* = \{10^{-5}$  to  $10^3\}$   $\mu\text{g m}^{-3}$ . The VBS distribution is based on a reference temperature of 298 K.



378 **3.5 Composition**

379 MCM+PRAM can be used to narrow down and compile a list of compounds playing a pivotal role in  
 380 contributing to SOA mass loadings and, also compare the relative importance of implementing PRAM  
 381 alongside the MCM. Figure 8 shows the most important compounds from both the MCM and PRAM that  
 382 condense on the seed particles and have a dominant contribution (>95%) to the  $\alpha$ -pinene ozonolysis SOA  
 383 mass loading at 293 K.



384 **Figure 8.** MCM and PRAM Compounds contributing to > 95 % of SOA mass at 293 K and 50ppb O<sub>3</sub> and  $\alpha$ -pinene concentrations.  
 385 At 293 K (Figure 8) the listed compounds (MCM+PRAM) contribute ~97 % to the SOA mass loading with  
 386 PRAM compounds contributing to ~48 % (of 97 %) in comparison to MCM compounds which contribute ~52  
 387 % (of 97%). On lowering the temperature to 258K the relative contributions of PRAM drop to 15 % (of ~98



388 %), while MCM dominates by contributing ~85 % (of ~98 %) respectively (Figure S3a). The contribution of  
389 PRAM increases to ~64 % (of ~97 %) and MCM contribution drops to 36 % (of ~97 %) at 313 K (Figure  
390 S3b). These results reflect the importance of PRAM as its contribution plays an increasingly dominant role  
391 with increasing temperatures and highlights the crucial few compounds that contribute to maximum SOA  
392 mass loadings for  $\alpha$ -pinene ozonolysis. The list of abundant compounds which together add up to contribute  
393 more than 95 % of SOA mass loadings at 258 K, 293 K and 313 K are presented in the supplement Table 1s  
394 (a, b & c). At 258 K MCM compounds namely pinonic acid ( $C_{10}H_{16}O_3$ , 4.4 %), C920PAN ( $C_{10}H_{15}NO_7$ , 9.3  
395 %), C108NO3 ( $C_{10}H_{15}NO_6$ , 8.9 %), C811PAN ( $C_9H_{13}NO_7$ , 10.1 %), C717NO3 ( $C_7H_9NO_6$ , 11.3 %) contribute  
396 significantly to the total SOA mass loadings while PRAM compounds such as  $C_{10}H_{14}O_7$  (0.88 %),  $C_{10}H_{16}O_4$   
397 (1.3 %),  $C_{10}H_{16}O_6$  (1.13 %) contribute significantly less. An increase in temperature to 293 K results in an  
398 overall increase in contribution by PRAM compounds, with  $C_{10}H_{14}O_{10}$  (3.6 %),  $C_{10}H_{14}O_{11}$  (6.2 %),  $C_{10}H_{16}O_{10}$   
399 (3.2 %) playing an important role in contributing to the SOA mass loadings. This trend of relative increase in  
400 the contribution by PRAM compounds over MCM compounds to SOA mass loadings is also evident as the  
401 temperatures are further increased to 313 K, where the PRAM compounds  $C_{10}H_{14}O_{11}$  (18.3 %),  $C_{10}H_{14}O_{12}$  (6  
402 %) and  $C_{10}H_{16}O_{12}$  (6.6 %) play a dominant role in increasing SOA mass loadings.

## 403 Conclusions

404 We simulated SOA mass yields derived from the oxidation of various BVOCs (isoprene,  $\alpha$ -pinene,  $\beta$ -  
405 pinene, limonene and  $\beta$ -caryophyllene), by the oxidants  $O_3$ , OH and  $NO_3$  using the zero-dimensional model  
406 MALTE-Box. The gas phase chemistry was simulated using the MCM in conjunction with PRAM. The aim  
407 was to verify the efficacy of MCM+PRAM in simulating the SOA mass yields. Additional simulations were  
408 performed to test the MCM+PRAM under varying temperature and NO concentrations. A few important  
409 compounds playing a major role in increasing the SOA mass yields for  $\alpha$ -pinene ozonolysis at different  
410 temperatures are also highlighted.

411 The simulations were designed to resemble ideal smog chambers experiments and experiments in  
412 oxidative flow reactors (OFR). No interactions between the gas phase and chamber walls were considered  
413 during the simulations. For the smog chamber setting, the standalone MCM generally under-predicts the mass  
414 yields obtained by the ozonolysis and OH oxidation of BVOCs. In contrast, the yields derived using  
415 MCM+PRAM for the smog chamber setup is in good agreement with the experimental results. For an  
416 idealized OFR setup, MCM+PRAM over-predicts the yields in case of ozonolysis and OH oxidation of  
417 BVOCs, while again the MCM under-predicts the SOA yields. This over prediction in mass yields for the  
418 OFR simulation was a result of higher CS used in the OFR. The relative contribution of HOM monomers and



419 dimers to the particle phase in OFR simulations is low when compared to the chamber simulations. This is  
420 due to higher RO<sub>2</sub> concentrations in OFR leading to termination of peroxy radical autoxidation, thereby  
421 affecting SOA yields. This needs to be considered when applying yields based on OFR simulations in  
422 regional or global chemical transport models

423 The BVOCs included in this study do not produce appreciable SOA mass yields when oxidized with  
424 NO<sub>3</sub>, as PRAM currently does not consider autoxidation of RO<sub>2</sub> formed from NO<sub>3</sub> oxidation of VOCs. This  
425 underlines the need for developing a NO<sub>3</sub> oxidation scheme which can better constrain and predict SOA mass  
426 yields. In accordance to the previous studies, the simulated SOA yields tend to decrease at higher  
427 temperatures. The PRAM contribution to mass yields at low temperatures (258.15 K) is ~14 %, which is  
428 substantially lower in comparison to MCM (~86 %). As the temperature is increased to 313.15 K, the  
429 contribution of PRAM to SOA mass yields begins to dominate over MCM. This most likely is due to MCM  
430 containing more SVOCs (compounds classified as SVOCs at 298 K), which show stronger contribution to  
431 particle phase at lower temperatures, due to decrease in saturation vapor pressures with temperature. It should  
432 be noted that the present temperature dependency of mass yields using PRAM are a first, and currently the  
433 best estimate in understanding the influence of temperature on the peroxy radical autoxidation formation. The  
434 simulated SOA yields with varying NO concentrations agree well with experimental results, i.e. SOA yields  
435 decrease with increasing NO concentrations due to the formation of more volatile compounds such as  
436 organonitrates and ketones.

437 Using PRAM in addition to MCM has paved way to bridge the gap in understanding the role and  
438 contribution of peroxy radical autoxidation to SOA formation. The variation of SOA yields for temperature  
439 and NO concentrations, indicates the limitations of global and regional models in predicting e.g. cloud  
440 condensation nuclei (CCN) effects using fixed SOA yields. The good agreement of modeled and experimental  
441 yields from smog chambers, respectively, could further help us parameterize the SOA yields, that could be  
442 applied at a global and regional model scale, to more accurately predict the direct and indirect impact of  
443 aerosol particles on e.g. radiation balance by aerosol scattering/absorption and CCN concentrations.

#### 444 **Author Contributions**

445 CX and MB served as the chief authors and editors of the paper. CX was performing the model simulations.  
446 The study was designed by CX, MB and PR. All other co-authors contributed to the analysis and writing of  
447 the paper.



449 **Acknowledgements**

450 The presented research has been funded by the Academy of Finland (Center of Excellence in Atmospheric  
451 Sciences) grant no. 4100104 and the Swedish Research Council FORMAS, project no. 2018-01745.

452 **References**

- 453 Ahlberg, E., Eriksson, A., Brune, W. H., Roldin, P. and Svenningsson, B.: Effect of salt seed particle surface  
454 area, composition and phase on secondary organic aerosol mass yields in oxidation flow reactors, *Atmos.*  
455 *Chem. Phys.*, 19(4), 2701–2712, doi:10.5194/acp-19-2701-2019, 2019.
- 456 Berndt, T., Richters, S., Jokinen, T., Hyttinen, N., Kurtén, T., Otkjær, R. V., Kjaergaard, H. G., Stratmann, F.,  
457 Herrmann, H., Sipilä, M., Kulmala, M. and Ehn, M.: Hydroxyl radical-induced formation of highly oxidized  
458 organic compounds, *Nat. Commun.*, 7(May), doi:10.1038/ncomms13677, 2016.
- 459 Bianchi, F., Garmash, O., He, X., Yan, C., Iyer, S., Rosendahl, I., Xu, Z., Rissanen, M. P., Riva, M., Taipale,  
460 R., Sarnela, N., Petäjä, T., Worsnop, D. R., Kulmala, M., Ehn, M. and Junninen, H.: The role of highly  
461 oxygenated molecules (HOMs) in determining the composition of ambient ions in the boreal forest, *Atmos.*  
462 *Chem. Phys.*, 17(22), 13819–13831, doi:10.5194/acp-17-13819-2017, 2017.
- 463 Bianchi, F., Kurtén, T., Riva, M., Mohr, C., Rissanen, M. P., Roldin, P., Berndt, T., Crouse, J. D.,  
464 Wennberg, P. O., Mentel, T. F., Wildt, J., Junninen, H., Jokinen, T., Kulmala, M., Worsnop, D. R., Thornton,  
465 J. A., Donahue, N., Kjaergaard, H. G. and Ehn, M.: Highly Oxygenated Organic Molecules (HOM) from Gas-  
466 Phase Autoxidation Involving Peroxy Radicals: A Key Contributor to Atmospheric Aerosol, *Chem. Rev.*,  
467 doi:10.1021/acs.chemrev.8b00395, 2019.
- 468 Bonn, B. and Moortgat, G. K.: New particle formation during  $\alpha$ - and  $\beta$ -pinene oxidation by O<sub>3</sub>, OH and NO<sub>3</sub>,  
469 and the influence of water vapour: Particle size distribution studies, *Atmos. Chem. Phys.*, 2(3), 183–196,  
470 doi:10.5194/acp-2-183-2002, 2002.
- 471 Boy, M., Hellmuth, O., Korhonen, H., Nilsson, E. D., Revelle, D., Turnipseed, A., Arnold, F. and Kulmala,  
472 M.: MALTE - Model to predict new aerosol formation in the lower troposphere, *Atmos. Chem. Phys.*, 6(12),  
473 4499–4517, doi:10.5194/acp-6-4499-2006, 2006.
- 474 Bruns, E. A., El Haddad, I., Keller, A., Klein, F., Kumar, N. K., Pieber, S. M., Corbin, J. C., Slowik, J. G.,  
475 Brune, W. H., Baltensperger, U. and Prévôt, A. S. H.: Inter-comparison of laboratory smog chamber and flow  
476 reactor systems on organic aerosol yield and composition, *Atmos. Meas. Tech.*, 8(6), 2315–2332,  
477 doi:10.5194/amt-8-2315-2015, 2015.
- 478
- 479 Chen, Q., Li, Y. L., McKinney, K. A., Kuwata, M. and Martin, S. T.: Particle mass yield from  $\beta$ -  
480 caryophyllene ozonolysis, *Atmos. Chem. Phys.*, 12(7), 3165–3179, doi:10.5194/acp-12-3165-2012, 2012.
- 481 Crouse, J. D. and Nielsen, L. B.: Autoxidation of Organic Compounds in the Atmosphere, *J. Phys. Chem.*  
482 *Lett.*, 24(4), 3513–3520, doi:10.1021/jz4019207, 2013.
- 483 Damian, V., Sandu, A., Damian, M., Potra, F. and Carmichael, G. R.: The kinetic preprocessor KPP - A  
484 software environment for solving chemical kinetics, *Comput. Chem. Eng.*, 26(11), 1567–1579,  
485 doi:10.1016/S0098-1354(02)00128-X, 2002.
- 486 Donahue, N. M., Robinson, A. L., Stanier, C. O. and Pandis, S. N.: Coupled Partitioning, Dilution, and  
487 Chemical Aging of Semivolatile Organics, *Environ. Sci. Technol.*, 40(8), 2635–2643, doi:10.1021/es052297c,  
488 2006.



- 489 Donahue, N. M., Robinson, A. L. and Pandis, S. N.: Atmospheric organic particulate matter: From smoke to  
490 secondary organic aerosol, *Atmos. Environ.*, 43(1), 94–106,  
491 doi:<https://doi.org/10.1016/j.atmosenv.2008.09.055>, 2009.
- 492 Donahue, N. M., Kroll, J. H., Pandis, S. N. and Robinson, A. L.: A two-dimensional volatility basis set-Part 2:  
493 Diagnostics of organic-aerosol evolution, *Atmos. Chem. Phys.*, 12(2), 615–634, doi:10.5194/acp-12-615-  
494 2012, 2012.
- 495 Draper, D. C., Farmer, D. K., Desyaterik, Y. and Fry, J. L.: A qualitative comparison of secondary organic  
496 aerosol yields and composition from ozonolysis of monoterpenes at varying concentrations of NO<sub>2</sub>, *Atmos.*  
497 *Chem. Phys.*, 15(21), 12267–12281, doi:10.5194/acp-15-12267-2015, 2015.
- 498 Ehn, M., Thornton, J. A., Kleist, E., Sipilä, M., Junninen, H., Pullinen, I., Springer, M., Rubach, F., Tillmann,  
499 R., Lee, B., Lopez-Hilfiker, F., Andres, S., Acir, I. H., Rissanen, M., Jokinen, T., Schobesberger, S.,  
500 Kangasluoma, J., Kontkanen, J., Nieminen, T., Kurtén, T., Nielsen, L. B., Jørgensen, S., Kjaergaard, H. G.,  
501 Canagaratna, M., Maso, M. D., Berndt, T., Petäjä, T., Wahner, A., Kerminen, V. M., Kulmala, M., Worsnop,  
502 D. R., Wildt, J. and Mentel, T. F.: A large source of low-volatility secondary organic aerosol, *Nature*,  
503 506(7489), 476–479, doi:10.1038/nature13032, 2014.
- 504 Friedman, B. and Farmer, D. K.: SOA and gas phase organic acid yields from the sequential photooxidation  
505 of seven monoterpenes, *Atmos. Environ.*, 187(January), 335–345, doi:10.1016/j.atmosenv.2018.06.003, 2018.
- 506 Fry, J. L., Kiendler-Scharr, A., Rollins, A. W., Brauers, T., Brown, S. S., Dorn, H. P., Dubé, W. P., Fuchs, H.,  
507 Mensah, A., Rohrer, F., Tillmann, R., Wahner, A., Wooldridge, P. J. and Cohen, R. C.: SOA from limonene:  
508 Role of NO<sub>3</sub> in its generation and degradation, *Atmos. Chem. Phys.*, 11(8), 3879–3894, doi:10.5194/acp-11-  
509 3879-2011, 2011.
- 510 Griffin, R. J.: Organic aerosol formation from the oxidation of biogenic hydrocarbons, , 104(D3), 3555–3567,  
511 1999.
- 512 Guenther, A., Baugh, B., Brasseur, G., Greenberg, J., Harley, P., Klinger, L., Serca, D., and Vierling, L.:  
513 Isoprene emission estimates and uncertainties for the Central African EXPRESSO study domain, *J. Geophys.*  
514 *Res. Atmos.*, 104(D23), 30625–30639, doi:10.1029/1999JD900391, 1999.
- 515 Guenther, A., Nicholas Hewitt, C., David, E., Fall, R., Chris, G., Tom, G., Peter, H., Klinger, L., Manuel, L.,  
516 McKay, W. A., Tom, P., Scholes, B., Steinbrecher, R., Tallamraju, R., Taylor, J. and Zimmerman, P.: A  
517 global model of natural volatile organic compound emissions s Raja the balance Triangle changes in the  
518 atmospheric accumulation rates of greenhouse Triangle Several inventories of natural and Exposure  
519 Assessment global scales have been two classes Fores, *J. Geophys. Res.*, 100(94), 8873–8892,  
520 doi:doi:10.1029/94JD02950, 1995.
- 521 Guenther, A., Geron, C., Pierce, T., Lamb, B., Harley, P. and Fall, R.: Natural emissions of non-methane  
522 volatile organic compounds, carbon monoxide, and oxides of nitrogen from North America, *Atmos. Environ.*,  
523 34(12–14), 2205–2230, doi:10.1016/S1352-2310(99)00465-3, 2000.
- 524 Hao, L. Q., Romakkaniemi, S., Yli-Pirilä, P., Joutsensaari, J., Kortelainen, A., Kroll, J. H., Miettinen, P.,  
525 Vaattovaara, P., Tiitta, P., Jaatinen, A., Kajos, M. K., Holopainen, J. K., Heijari, J., Rinne, J., Kulmala, M.,  
526 Worsnop, D. R., Smith, J. N. and Laaksonen, A.: Mass yields of secondary organic aerosols from the  
527 oxidation of  $\alpha$ -pinene and real plant emissions, *Atmos. Chem. Phys.*, 11(4), 1367–1378, doi:10.5194/acp-11-  
528 1367-2011, 2011.
- 529 Henry, K. M., Lohaus, T. and Donahue, N. M.: Organic Aerosol Yields from  $\alpha$ -Pinene Oxidation: Bridging  
530 the Gap between First-Generation Yields and Aging Chemistry, *Environ. Sci. Technol.*, 46(22), 12347–  
531 12354, doi:10.1021/es302060y, 2012.





- 532 Jacobson, M. Z.: Numerical techniques to solve condensational and dissolutional growth equations when  
533 growth is coupled to reversible reactions, *Aerosol Sci. Technol.*, 27(4), 491–498,  
534 doi:10.1080/02786829708965489, 1997.
- 535 Jenkin, M. E., Saunders, S. M. and Pilling, M. J.: The tropospheric degradation of volatile organic  
536 compounds: A protocol for mechanism development, *Atmos. Environ.*, 31(1), 81–104, doi:10.1016/S1352-  
537 2310(96)00105-7, 1997.
- 538 Jenkin, M. E., Young, J. C. and Rickard, A. R.: The MCM v3.3.1 degradation scheme for isoprene, *Atmos.*  
539 *Chem. Phys.*, 15(20), 11433–11459, doi:10.5194/acp-15-11433-2015, 2015.
- 540 Jenkin, M. E., Wyche, K. P., Evans, C. J., Carr, T., Monks, P. S., Alfarra, M. R., Barley, M. H., McFiggans,  
541 G. B., Young, J. C. and Rickard, A. R.: Development and chamber evaluation of the MCM v3.2 degradation  
542 scheme for  $\beta$ -caryophyllene, *Atmos. Chem. Phys.*, 12(11), 5275–5308, doi:10.5194/acp-12-5275-2012, 2012.
- 543 Jenkin, M. E., Valorso, R., Aumont, B. and Rickard, A. R.: Estimation of rate coefficients and branching ra-  
544 tios for reactions of organic peroxy radicals for use in automated mechanism construction, *Atmos. Chem.*  
545 *Phys. Discuss.*, (February), 1–46, doi:10.5194/acp-2019-44, 2019.
- 546 Jokinen, T., Berndt, T., Makkonen, R., Kerminen, V.-M., Junninen, H., Paasonen, P., Stratmann, F.,  
547 Herrmann, H., Guenther, A. B., Worsnop, D. R., Kulmala, M., Ehn, M. and Sipilä, M.: Production of  
548 extremely low volatile organic compounds from biogenic emissions: Measured yields and atmospheric  
549 implications, *Proc. Natl. Acad. Sci.*, 112(23), 7123–7128, doi:10.1073/pnas.1423977112, 2015.
- 550 Kanakidou, M., Seinfeld, J. H., Pandis, S. N., Barnes, I., Dentener, F. J., Facchini, M. C. and Dingenen, R.  
551 Van: Organic aerosol and global climate modelling: a review, , 1053–1123, 2005.
- 552 Kang, E. and Root, M. J.: Introducing the concept of Potential Aerosol Mass (PAM), *Atmos. Chem. Phys.*,  
553 (7), 5727–5744
- 554 Keywood, M. D., Varutbangkul, V., Bahreini, R., Flagan, R. C. and Seinfeld, J. H.: Secondary organic aerosol  
555 formation from the ozonolysis of cycloalkenes and related compounds, *Environ. Sci. Technol.*, 38(15), 4157–  
556 4164, doi:10.1021/es035363o, 2004.
- 557 Korhonen, H., Lehtinen, K. E. J. and Kulmala, M.: Atmospheric Chemistry and Physics Multicomponent  
558 aerosol dynamics model UHMA: model development and validation, *Atmos. Chem. Phys.*, 4, 757–771,  
559 doi:10.1002/erv.2305, 2004.
- 560 Kristensen, K., Cui, T., Zhang, H., Gold, A., Glasius, M. and Surratt, J. D.: Dimers in  $\alpha$ -pinene secondary  
561 organic aerosol: Effect of hydroxyl radical, ozone, relative humidity and aerosol acidity, *Atmos. Chem. Phys.*,  
562 14(8), 4201–4218, doi:10.5194/acp-14-4201-2014, 2014.
- 563 Kristensen, K., Jensen, L. N., Glasius, M. and Bilde, M.: The effect of sub-zero temperature on the formation  
564 and composition of secondary organic aerosol from ozonolysis of alpha-pinene, *Environ. Sci. Process.*  
565 *Impacts*, 19(10), 1220–1234, doi:10.1039/c7em00231a, 2017.
- 566 Kroll, J. H., Ng, N. L., Murphy, S. M., Flagan, R. C. and Seinfeld, J. H.: Secondary organic aerosol formation  
567 from isoprene photooxidation under high-NO<sub>x</sub> conditions, *Geophys. Res. Lett.*, 32(18), 1–4,  
568 doi:10.1029/2005GL023637, 2005.
- 569 Lambe, A. T., Onasch, T. B., Massoli, P., Croasdale, D. R., Wright, J. P., Ahern, A. T., Williams, L. R.,  
570 Worsnop, D. R., Brune, W. H. and Davidovits, P.: Laboratory studies of the chemical composition and cloud  
571 condensation nuclei (CCN) activity of secondary organic aerosol (SOA) and oxidized primary organic aerosol  
572 (OPOA), *Atmos. Chem. Phys.*, 11(17), 8913–8928, doi:10.5194/acp-11-8913-2011, 2011.



- 573 Lambe, A. T., Chhabra, P. S., Onasch, T. B., Brune, W. H., Hunter, J. F., Kroll, J. H., Cummings, M. J.,  
574 Brogan, J. F., Parmar, Y., Worsnop, D. R., Kolb, C. E. and Davidovits, P.: Effect of oxidant concentration,  
575 exposure time, and seed particles on secondary organic aerosol chemical composition and yield, *Atmos.*  
576 *Chem. Phys.*, 15(6), 3063–3075, doi:10.5194/acp-15-3063-2015, 2015.
- 577 Lee, A., Goldstein, A. H., Keywood, M. D., Gao, S., Varutbangkul, V., Bahreini, R., Ng, N. L., Flagan, R. C.  
578 and Seinfeld, J. H.: Gas-phase products and secondary aerosol yields from the ozonolysis of ten different  
579 terpenes, *J. Geophys. Res. Atmos.*, 111(7), 1–18, doi:10.1029/2005JD006437, 2006.
- 580 Liu, J., D’Ambro, E. L., Lee, B. H., Lopez-Hilfiker, F. D., Zaveri, R. A., Rivera-Rios, J. C., Keutsch, F. N.,  
581 Iyer, S., Kurten, T., Zhang, Z., Gold, A., Surratt, J. D., Shilling, J. E. and Thornton, J. A.: Efficient Isoprene  
582 Secondary Organic Aerosol Formation from a Non-IEPOX Pathway, *Environ. Sci. Technol.*, 50(18), 9872–  
583 9880, doi: 10.1021/acs.est.6b01872, 2016.
- 584 Miller, K. A., Siscovick, D. S., Sheppard, L., Shepherd, K., Sullivan, J. H., Anderson, G., L. and Kaufman J.  
585 D.: Long-Term Exposure to Air Pollution and Incidence of Cardiovascular Events in Women, *N. Engl. J.*  
586 *Med.*, 356(5), 447–458, doi:10.1002/anie.201206370, 2007.
- 587 Nannoolal, Y., Rarey, J. and Ramjugernath, D.: Estimation of pure component properties part 3. Estimation of  
588 the vapor pressure of non-electrolyte organic compounds via group contribution and group interactions, *Fluid*  
589 *Phase Equilib.*, 269(1–2), 117–133, doi: 10.1016/j.fluid.2008.04.020, 2008.
- 590 Nah, T., Sanchez, J., Boyd, C. M. and Ng, N. L.: Photochemical Aging of  $\alpha$ -pinene and  $\beta$ -pinene Secondary  
591 Organic Aerosol formed from Nitrate Radical Oxidation, *Environ. Sci. Technol.*, 50(1), 222–231,  
592 doi:10.1021/acs.est.5b04594, 2016.
- 593 Ng, N. L. and Chhabra, P. S.: Effect of NO<sub>x</sub> level on secondary organic aerosol (SOA) formation from the  
594 photooxidation of terpenes, *Atmos. Chem. Phys.*, (7), 5159–5174, doi: 10.1016/j.cub.2015.10.018, 2007.
- 595 Pankow, J. F. and Asher, W. E.: SIMPOL.1: a simple group contribution method for predicting vapor  
596 pressures and enthalpies of vaporization of multifunctional organic compounds, *Rev. Mex. Ciencias Farm.*,  
597 (8), 2773–2796, doi:doi: 10.5194/acp-8-2773-2008, 2008.
- 598 Pathak, R., Donahue, N. M. and Pandis, S. N.: Ozonolysis of  $\beta$ -pinene: Temperature dependence of secondary  
599 organic aerosol mass fraction, *Environ. Sci. Technol.*, 42(14), 5081–5086, doi:10.1021/es070721z, 2008.
- 600 Pathak, R. K., Stanier, C. O., Donahue, N. M. and Pandis, S. N.: Ozonolysis of  $\alpha$ -pinene at atmospherically  
601 relevant concentrations: Temperature dependence of aerosol mass fractions (yields), *J. Geophys. Res. Atmos.*,  
602 112(3), 1–8, doi:10.1029/2006JD007436, 2007.
- 603 Presto, A. A., Huff Hartz, K. E. and Donahue, N. M.: Secondary organic aerosol production from terpene  
604 ozonolysis. 2. Effect of NO<sub>x</sub> concentration, *Environ. Sci. Technol.*, 39(18), 7046–7054,  
605 doi:10.1021/es050400s, 2005.
- 606 Quéléver, L. L. J., Kristensen, K., Jensen, L., Rosati, B., Teiwes, R., Daellenbach, K. R., Peräkylä, O., Roldin,  
607 P., Pedersen, H. B., Glasius, M., Bilde, M., and Ehn, M.: Effect of temperature on the formation of Highly-  
608 oxygenated Organic Molecules (HOM) from alpha-pinene ozonolysis, *Atmos. Chem. Phys. Discuss.*,  
609 <https://doi.org/10.5194/acp-2018-1276>, in review, 2018.
- 610 Roldin P., Ehn, M., Kurtén, T., Olenius, T., Rissanen, M.P., Sarnela, N., Elm, J., Rantala, P., Hao, L.,  
611 Hyttinen, N., Heikkinen, L., Worsnop, D. R., Pichelstorfer, L., Xavier, C., Clusius, P., Öström, E., Petäjä, T.,  
612 Kulmala, M., Vehkamäki, H., Virtanen, A., Riipinen, I., and Boy, M., The role of highly oxygenated organic  
613 molecules in the Boreal aerosol-cloud-climate system, *Nature Communications*, under review 2019.



- 614 Rosenfeld, D., Andreae, M. O., Asmi, A., Chin M., De Leeuw, G., Donovan, D. P., Kahn, R, Kinne, S.,  
615 Kivekäs, N., Kulmala, M., Lau W., Schmidt K, S., Suni T., Wagner T., Wild, M., and Quaas J., Global obser-  
616 vations of aerosol-cloud-precipitation-climate interactions, *Rev. Geophys.*, 52, 750–808,  
617 doi:10.1002/2013RG000441.
- 618 Saathoff, H. and Naumann, K.-H.: Temperature dependence of yields of secondary organic aerosols from the  
619 ozonolysis of  $\alpha$ -pinene and limonene, *Atmos. Chem. Phys.*, (March), 4–15, doi:10.5194/acp-9-1551-2009,  
620 2009.
- 621 Sarrafzadeh, M., Wildt, J., Pullinen, I., Springer, M., Kleist, E., Tillmann, R., Schmitt, S. H., Wu, C., Mentel,  
622 T. F., Zhao, D., Hastie, D. R. and Kiendler-Scharr, A.: Impact of NO<sub>x</sub> and OH on secondary organic aerosol  
623 formation from  $\beta$ -pinene photooxidation, *Atmos. Chem. Phys.*, 16(17), 11237–11248, doi:10.5194/acp-16-  
624 11237-2016, 2016.
- 625 Saunders, S. M., Jenkin, M. E., Derwent, R. G. and Pilling, M. J.: Protocol for the development of the Master  
626 Chemical Mechanism, MCM v3 (Part A): Tropospheric degradation of non-aromatic volatile organic  
627 compounds, *Atmos. Chem. Phys.*, 3(1), 161–180, doi:10.5194/acp-3-161-2003, 2003.
- 628 Schmale, J., Henning, S., Henzing, B., Keskinen, H., Sellegri, K., Ovadnevaite, J., Bougiatioti, A., Kalivitis,  
629 N., Stavroulas, I., Jefferson, A., Park, M., Schlag, P., Kristensson, A., Iwamoto, Y., Pringle, K., Reddington,  
630 C., Aalto, P., Äijälä, M., Baltensperger, U., Bialek, J., Birmili, W., Bukowiecki, N., Ehn, M., Fjæraa, A. M.,  
631 Fiebig, M., Frank, G., Fröhlich, R., Frumau, A., Furuya, M., Hammer, E., Heikkinen, L., Herrmann, E.,  
632 Holzinger, R., Hyono, H., Kanakidou, M., Kiendler-Scharr, A., Kinouchi, K., Kos, G., Kulmala, M.,  
633 Mihalopoulos, N., Motos, G., Nenes, A., O’Dowd, C., Paramonov, M., Petäjä, T., Picard, D., Poulain, L.,  
634 Prévôt, A. S. H., Slowik, J., Sonntag, A., Swietlicki, E., Svenningsson, B., Tsurumaru, H., Wiedensohler, A.,  
635 Wittbom, C., Ogren, J. A., Matsuki, A., Yum, S. S., Myhre, C. L., Carslaw, K., Stratmann, F. and Gysel, M.:  
636 Corrigendum: Collocated observations of cloud condensation nuclei, particle size distributions, and chemical  
637 composition, *Sci. data*, 5, 180094, doi:10.1038/sdata.2018.94, 2018.
- 638 Shilling, J. E.: Particle mass yield in secondary organic aerosol formed by the dark ozonolysis of  $\alpha$ -pinene,  
639 *Atmos. Chem. Phys.*, 8(1992), 2073–2088, 2008.
- 640 Stirnweis, L., Marcolli, C., Dommen, J., Barmet, P., Frege, C., Platt, S. M., Bruns, E. A., Krapf, M., Slowik,  
641 J. G., Wolf, R., Prévôt, A. S. H., Baltensperger, U. and El-Haddad, I.: Assessing the influence of NO<sub>x</sub> con-  
642 centrations and relative humidity on secondary organic aerosol yields from  $\alpha$ -pinene photo-oxidation through  
643 smog chamber experiments and modelling calculations, *Atmos. Chem. Phys.*, 17(8), 5035–5061, doi:10.5194/  
644 acp-17-5035-2017, 2017.
- 645 Tasoglou, A. and Pandis, S. N.: Formation and chemical aging of secondary organic aerosol during the  $\beta$ -  
646 caryophyllene oxidation, *Atmos. Chem. Phys.*, 15(11), 6035–6046, doi:10.5194/acp-15-6035-2015, 2015.
- 647 Topping, D.: UManSysProp v1.0: an online and open-source facility for molecular property prediction and  
648 atmospheric aerosol calculations, , 899–914, doi:10.5281/zenodo.45143, 2016.
- 649 Waring, M. S.: Secondary organic aerosol formation by limonene ozonolysis: Parameterizing multi-  
650 generational chemistry in ozone- and residence time-limited indoor environments, *Atmos. Environ.*, 144, 79–  
651 86, doi:https://doi.org/10.1016/j.atmosenv.2016.08.051, 2016.
- 652 Zhao, D., Schmitt, S. H., Wang, M., Acir, I. H., Tillmann, R., Tan, Z., Novelli, A., Fuchs, H., Pullinen, I.,  
653 Wegener, R., Rohrer, F., Wildt, J., Kiendler-Scharr, A., Wahner, A. and Mentel, T. F.: Effects of NO<sub>x</sub> and  
654 SO<sub>2</sub> on the secondary organic aerosol formation from photooxidation of  $\alpha$ -pinene and limonene, *Atmos.*  
655 *Chem. Phys.*, 18(3), 1611–1628, doi:10.5194/acp-18-1611-2018, 2018.



656 Zhao, D. F., Kaminski, M., Schlag, P., Fuchs, H., Acir, I. H., Bohn, B., Häseler, R., Kiendler-Scharr, A.,  
657 Rohrer, F., Tillmann, R., Wang, M. J., Wegener, R., Wildt, J., Wahner, A. and Mentel, T. F.: Secondary  
658 organic aerosol formation from hydroxyl radical oxidation and ozonolysis of monoterpenes, *Atmos. Chem.*  
659 *Phys.*, 15(2), 991–1012, doi:10.5194/acp-15-991-2015, 2015.